

Hydrothermal Construction of Magnetic Z-Scheme N-BiOBr/NiFe₂O₄ Nanocomposite with Enhanced Sunlight-Driven Industrial Textile Effluent Degradation

Jin-Chung Sin^{1,3}, Sze-Mun Lam^{2,3}, Honghu Zeng³

¹Department of Petrochemical Engineering, Faculty of Engineering and Green Technology, Universiti Tunku Abdul Rahman, Jalan Universiti, Bandar Barat, 31900 Kampar, Perak, Malaysia
First.sinjc@utar.edu.my

²Department of Environmental Engineering, Faculty of Engineering and Green Technology, Universiti Tunku Abdul Rahman, Jalan Universiti, Bandar Barat, 31900 Kampar, Perak, Malaysia
Second.lamsm@utar.edu.my

³College of Environmental Science and Engineering, Guilin University of Technology, Guilin 541004, China
Third.zenghonghu@glut.edu.cn

Abstract - Z-scheme N-BiOBr/NiFe₂O₄ (NBO/NFO) nanocomposite as a sunlight-responsive photocatalyst was fabricated via a hydrothermal route. The results showed that NFO nanoparticles were well deposited on NBO nanosheets. The fabricated nanocomposite exhibited good magnetic property, which enabled the easy solid-liquid separation. The intimate contact between both semiconductors significantly improved the charge carrier separation by recombining the electron in conduction band of NBO with hole in valence band of NFO. The remained electron and hole in respective semiconductor displayed strong redox ability to initiate the photoreaction. Thus, the NBO/NFO showed the highest photoactivity in degrading textile effluent. The hydroxyl radicals contributed majorly in the photodegradation process. The present study showed that the NBO/NFO was an effective candidate for environmental remediation applications.

Keywords: N-doped BiOBr/NiFe₂O₄, Z-scheme heterojunction, Photodegradation, Industrial textile effluent

1. Introduction

Over the past few years, BiOBr has attracted lots of attention as significant photocatalyst due to its unique layer structure, high photostability and ease of availability. Nevertheless, the weak sunlight absorption, quick charge carrier recombination and poor catalyst recovery tremendously impeded its commercial applications [1,2]. Doping the BiOBr with nonmetallic species has been shown as an effective route to improve the visible light absorption [2]. Nitrogen atom with a similar atomic radius to oxygen atom was indeed an excellent dopant to induce a wider range of optical absorption by altering the band structure of semiconductor. Additionally, fabricating Z-scheme photocatalyst by suitably interfacing two single semiconductors is an efficacious approach to accelerate the charge carrier separation [3]. The NiFe₂O₄ is one of the widely examined photocatalysts because of its exceptional superparamagnetic ability and high visible light absorption [4]. Herein, the Z-scheme N-BiOBr/NiFe₂O₄ (NBO/NFO) heterostructure was hydrothermally fabricated by decorating the NFO nanoparticles on NBO nanosheets. The photoactivities were evaluated by textile effluent degradation. A Z-scheme photocatalysis was proposed and validated, which was accountable for improved photocatalytic performance. To our knowledge, there is no available study on textile effluent degradation with recyclable magnetic NBO/NFO nanocomposite.

2. Experimental

2.1. Fabrication of NBO nanosheets

2.425 g Bi(NO₃)₃·5H₂O and 0.6 g urea were dissolved in 150 mL deionized water, then 0.595 g KBr was dissolved in the above solution. The resulting mixture was hydrothermally treated in a Teflon-lined autoclave at 180°C for 12 h. The precipitates from the reaction mixture were collected by filtration, washed with deionized water for 5 times and dried at 80°C for 24 h. Using the identical hydrothermal synthesis, pristine BiOBr (BO) was also fabricated except the addition of urea.

2.2. Fabrication of NBO/NFO nanocomposite

0.296 g of $\text{Ni}(\text{NO}_3)_2 \cdot 6\text{H}_2\text{O}$ and 0.550 g of $\text{FeCl}_3 \cdot 6\text{H}_2\text{O}$ were dissolved in 150 mL deionized water. The pH of the mixture was then adjusted to 12.0 using 2 M NaOH solution. Subsequently, 1.0 g of as-fabricated NBO was added into the above suspension and ultrasonically dispersed for 60 min. The resulting mixture was then hydrothermally treated in a Teflon-lined autoclave at 180°C for 12 h. The precipitates from the reaction mixture were collected by filtration, washed with deionized water for 5 times, dried at 80°C for 24 h and finally calcined at 500°C for 2 h. The NFO nanoparticle was also fabricated via the same method except the addition of NBO.

2.3. Characterization of as-fabricated samples

The as-fabricated samples were characterized using field-emission scanning electron microscopy (FESEM, Quanta FEG 450), transmission electron microscopy (TEM, Philips CM 12), high-resolution transmission electron microscopy (HRTEM, Tecnai 20), X-ray diffraction (XRD, Philips PW1820), vibrating sample magnetometer (VSM, Quantum Design MPMS-5S), UV-vis diffuse reflectance spectroscopy (UV-vis DRS, Perkin Elmer Lambda 35), photoluminescence spectroscopy (PL, Perkin Elmer Lambda S55), transient photocurrent response (Gamry Interface 1000 electrochemical workstation) and electron spin resonance (ESR, Bruker ESR JES-FA200 spectrometer).

2.4. Photocatalytic performance

For photoactivity evaluation, the effluent was taken from a textile industry (Penang, Malaysia). Typically, 1.0 g/L photocatalyst was suspended in 200 mL textile effluent with a concentration of 100 mg/L. The suspension was exposed to sunlight irradiation after equilibrated in dark for 1 h. At certain time intervals, aliquots were sampled and analyzed with chemical oxygen demand (COD). Additionally, the colour of solution was determined using a UV-vis spectrophotometer. The hydroxyl ($\bullet\text{OH}$) radical, holes (h^+), superoxide anion ($\text{O}_2\bullet^-$) radical and H_2O_2 were scavenged by isopropanol (IPA, 1 mM), ethylene diaminetetraacetic acid (EDTA, 1 mM), benzoquinone (BQ, 1 mM) and catalase (100 units/mL), respectively [5,6].

3. Results and Discussion

The FESEM images of BO and NBO displayed nanosheet morphology with sizes of 1-4 μm (Fig. 1 a-b). The NFO demonstrated irregular spherical particle with sizes of 20-400 nm (Fig. 1c). For NBO/NFO, the FESEM and TEM analyses showed that the NFO nanoparticles were well deposited on NBO nanosheets (Fig. 1d-e). The size distribution and morphology of NBO and NFO were also maintained during constructing the NBO/NFO which was developed via self-assembly. The intimate interface in the nanocomposite was noticed via HRTEM image (Fig. 1f), which was in favor of charge separation and migration. The lattice spacing of 0.28 and 0.25 nm corresponded to the crystal planes of NBO and NFO, respectively, which verified the formation of heterostructure photocatalyst. The process for the formation of NBO/NFO is illustrated in Fig. 1g.

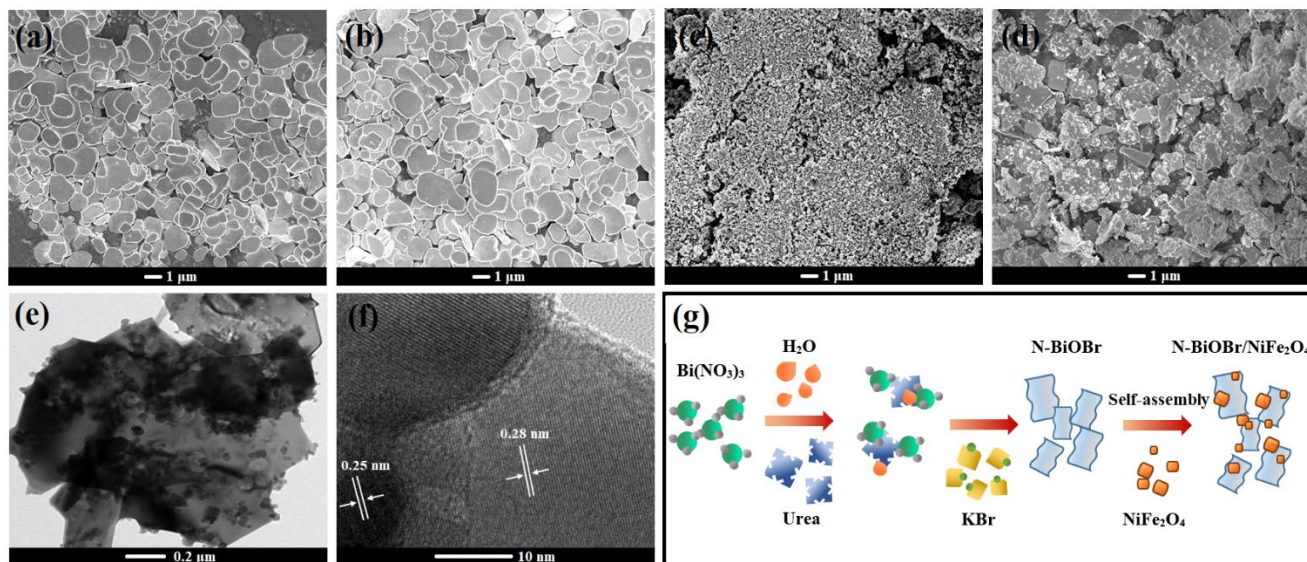


Fig. 1: FESEM images of (a) BO, (b) NBO, (c) NFO and (d) NBO/NFO. (e) TEM and (f) HRTEM images of NBO/NFO. (g) Schematic diagram showing formation of NBO/NFO.

The XRD patterns are depicted in Fig. 2a, from which it can be determined that all the diffraction peaks of BO were indexed to tetragonal structure (JCPDS no. 09-0393). Additionally, N-doping did not demonstrate any effect on the overall crystalline structure of BO. For NFO, the diffraction peaks were well corresponded to cubic crystal phase (JCPDS no. 54-0964). Diffraction peaks of tetragonal BO and cubic NFO were discovered in as-fabricated nanocomposite, which further confirmed the successful production of NBO/NFO. No other diffraction peaks arising from impurities were identified, suggesting the purity of fabricated photocatalysts. The magnetization curve in Fig. 2b demonstrated the superparamagnetic behavior of NBO/NFO that was favorable for practical environmental applications. Moreover, it was very convenient to separate the nanocomposite from the solution using a magnet (inset of Fig. 2b). In Fig. 2c, the UV-vis DRS spectrum of corresponding BO showed an absorption edge at 417 nm, whereas the NFO had a stronger absorption in longer wavelengths with an absorption edge of 600 nm. Additionally, N-doping provided impurity levels occurring in between the band gap of BO which led to small red shift in the optical absorption. Decoration of NFO enhanced the light absorption of NBO, indicating the formation of heterojunction between semiconductors. Based on Tauc plot, the band gap energies of BO, NFO, NBO and NBO/NFO were 2.97, 2.04, 2.89 and 2.86 eV, respectively (Fig. 2d). The conduction band (E_{CB}) of NBO and NFO were calculated as 0.47 and 0.32 eV, and the valence band (E_{VB}) were 3.36 and 2.36 eV, respectively, using the Mulliken electronegativity theory [5].

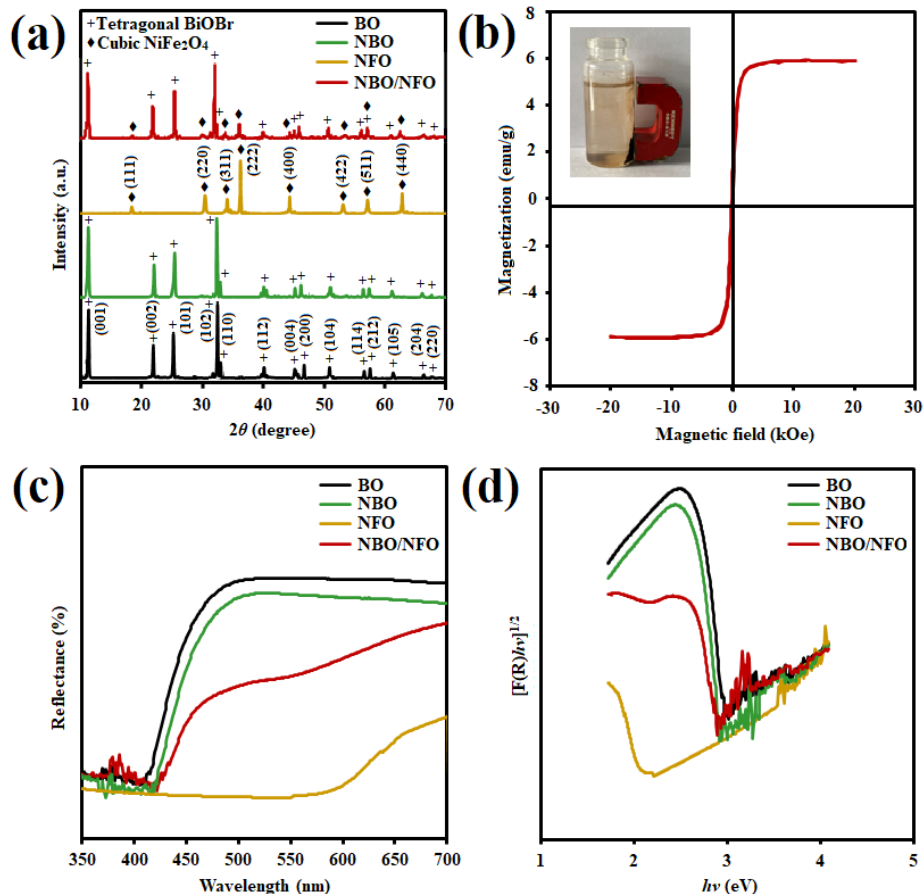


Fig. 2: (a) XRD patterns of as-fabricated samples. (b) Magnetization curve of NBO/NFO. (c) UV-vis DRS spectra and (d) Tauc plots of as-fabricated samples.

Fig. 3a shows the photodegradation of textile effluent over as-fabricated samples. As noticed, dark adsorption and direct photolysis contributed to negligible decay of textile effluent. After 180 min of sunlight irradiation, the COD reduction of BO, NBO, NFO and NBO/NFO were 47.5, 63.1, 37.8 and 94.4%, respectively. Meanwhile, the physical mixture of NBO and NFO (NBO + NFO) only degraded 51.2% of textile effluent at the same duration. The recorded photoactivity of NBO/NFO was also higher than the previously reported photocatalysts on textile effluent degradation [7,8]. For instance, the photodegradation efficiency was 89.3% after 180 min in Ref. [7] and approximately 20% after 360 min in Ref. [8]. The superb photoactivity can be ascribed to the heterojunction formed by merging two photocatalysts, leading to enhanced charge carrier separation and interfacial charge transfer. Moreover, the improved photoactivity of nanocomposite can be further validated by color removal. Complete color removal was found for NBO/NFO, which was noticeably higher than those of BO (77.2%), NBO (97.8%), NFO (48.9%) and NBO + NFO (82.7%) (Fig. 3b).

The PL spectra of fabricated materials are displayed in Fig. 3c. All single photocatalysts showed stronger PL intensity, which indicated the fast charge carrier recombination. Conversely, the NBO/NFO possessed the weakest PL intensity, revealing the electron-hole (e^-h^+) separation has been accelerated via charge transition between NBO and NFO. To further support this, transient photocurrent response was performed (Fig. 3d). The photocurrent for NBO/NFO was much higher than the single photocatalysts, validating the importance of Z-scheme heterojunction in preventing the charge carrier recombination. The principal reactive species that responsible for textile effluent degradation were determined via the radical trapping tests. As shown in Fig. 3e, the photoreaction was insignificantly inhibited by adding

BQ, while slightly affected with EDTA and catalase. However, the photodegradation restrained severely when IPA was introduced, implying that the $\bullet\text{OH}$ rather than H_2O_2 , h^+ and $\text{O}_2^{\bullet-}$ was the dominant reactive species to degrade textile effluent. Moreover, ESR analysis was conducted to identify the $\bullet\text{OH}$ (inset of Fig. 3e). Four major characteristic peaks of DMPO- $\bullet\text{OH}$ were detected, proving the formation and participation of $\bullet\text{OH}$ in the photodegradation reaction.

Based on above results, the improved textile effluent degradation over NBO/NFO can be explained via Z-scheme heterojunction mechanism (Fig. 3f). Under sunlight irradiation, the photoinduced e^- were excited from VB to CB for both photocatalysts. The VB potential of NBO was more positive than the NFO, whereas the CB potential of NFO was more negative than that of NBO. In this incident, the e^- in CB of NBO with lower potential can easily transfer and recombined with the h^+ in VB of NFO, which facilitated the e^-h^+ pairs separation. The CB of NFO was more negative than the +0.682 eV/NHE ($\text{O}_2/\text{H}_2\text{O}_2$) revealing that the accumulated e^- with stronger reducibility can reduce O_2 to form H_2O_2 . It was also worth noting that the CB of NFO was not negative enough to create $\text{O}_2^{\bullet-}$ via O_2 reduction ($E^\circ(\text{O}_2/\text{O}_2^{\bullet-}) = -0.33$ eV), which was compatible with the findings of radical trapping test. Conversely, the VB of NBO was positive enough compared to 2.38 eV/NHE ($\text{OH}^-/\bullet\text{OH}$) and 2.72 eV/NHE ($\text{H}_2\text{O}/\bullet\text{OH}$) so the photoinduced h^+ with strong oxidizability can react with OH^- or H_2O oxidizing them into $\bullet\text{OH}$. The resulting $\bullet\text{OH}$ generated on nanocomposite being highly oxidizing agents and favored the organics degradation [5-7]. Obviously, the Z-scheme heterojunction promoted the charge transfer and reserved strong redox capability for photodegradation. Subsequently, improved the yield of $\bullet\text{OH}$ in the textile effluent degradation, which undeniably boosted the photoactivity of NBO/NFO.

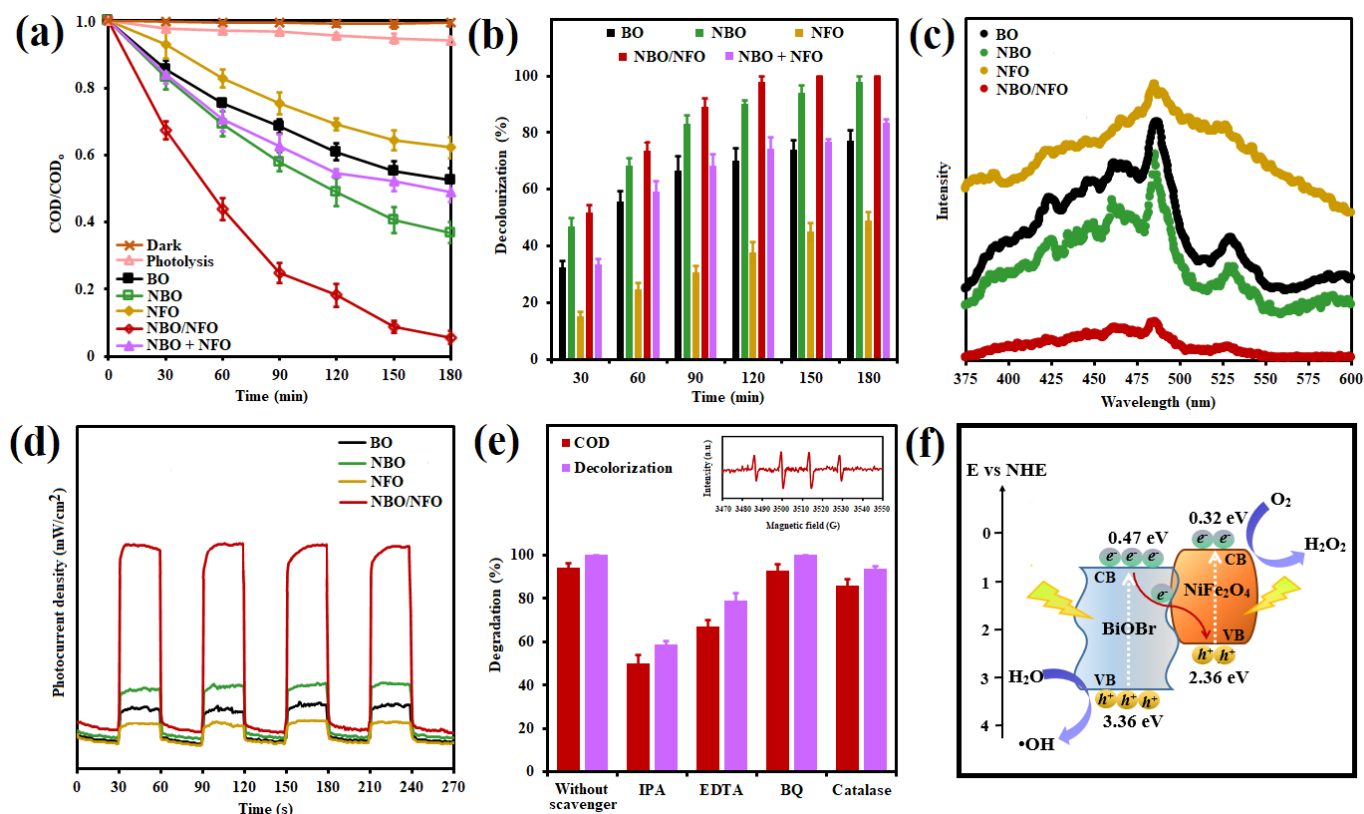


Fig. 3: Photocatalytic (a) COD reduction and (b) Color removal of textile effluent. (c) PL spectra and (d) Photocurrent response of as-fabricated samples. (e) Reactive species analysis and (f) Z-scheme photocatalysis over NBO/NFO.

4. Conclusion

In summary, we have fabricated the Z-scheme NBO/NFO nanocomposite using a surfactant-free hydrothermal technique. The fabricated nanocomposite displayed excellent solar photodegradation of textile effluent. The well-scheme heterojunction enhanced the photoactivity of nanocomposite by expediting the separation and curtailing the recombination of charge carriers. The •OH was principal reactive species in photodegradation reaction. The overall revealed that the NBO/NFO can be a superior sunlight-driven photocatalyst for environmental pollution control.

Acknowledgements

This research was supported by Ministry of Higher Education (MoHE) through Fundamental Research Grant Scheme (FRGS/1/2019/TK02/UTAR/02/4 and FRGS/1/2022/TK08/UTAR/02/5). We also want to thank to the Universiti Tunku Abdul Rahman (UTARRF/2021-C2/L03), Research funds of The Guangxi Key Laboratory of Theory and Technology for Environmental Pollution Control, China (1801K012 and 1801K013), ASEAN Young Talented Scientist Program of Guangxi and special funding for Guangxi “Bagui Scholar” construction project for sponsoring this work.

References

- [1] Y. L. Ling, Y. Z. Dai, “Direct Z-scheme hierarchical WO_3/BiOBr with enhanced photocatalytic degradation performance under visible light,” *Appl. Surf. Sci.*, vol. 509, pp. 145201, 2020.
- [2] C. Y. Wang, Q. Zeng, G. C. Zhu, “Novel S-doped BiOBr nanosheets for the enhanced photocatalytic degradation of bisphenol A under visible light irradiation,” *Chemosphere*, vol. 268, pp. 128854, 2021.
- [3] K. Xu, J. Feng, “Superior photocatalytic performance of $\text{LaFeO}_3/\text{g-C}_3\text{N}_4$ heterojunction nanocomposites under visible light irradiation,” *RSC Adv.*, vol. 7, pp. 45369-45376, 2017.
- [4] Y. Wang, H. Wang, Y. Yang, B. F. Xin, “Magnetic NiFe_2O_4 3D nanosphere photocatalyst: Glycerol-assisted microwave solvothermal synthesis and photocatalytic activity under microwave electrodeless discharge lamp,” *Ceram. Int.*, vol. 47, pp. 14594-14602, 2021.
- [5] J. C. Sin, S. M. Lam, H. H. Zeng, H. Lin, H. X. Li, A. R. Mohamed, “Constructing magnetic separable $\text{BiOBr}/\text{MnFe}_2\text{O}_4$ as efficient Z-scheme nanocomposite for visible light-driven degradation of palm oil mill effluent and inactivation of bacteria,” *Mater. Lett.*, vol. 275, pp. 128112, 2020.
- [6] Y. H. Chin, J. C. Sin, S. M. Lam, A. R. Mohamed, “Preparation of Nb_2O_5 -decorated hierarchical porous ZnO microspheres with enhanced photocatalytic degradation of palm oil mill effluent,” *J. Mater. Sci.: Mater. Electron.*, vol. 30, pp. 1739-1750, 2019.
- [7] A. Fouda, S. E. Hassan, E. Saied, M. F. Hamza, “Photocatalytic degradation of real textile and tannery effluent using biosynthesized magnesium oxide nanoparticles (MgO-NPs), heavy metal adsorption, phytotoxicity, and antimicrobial activity,” *J. Environ. Chem. Eng.*, vol. 9, pp. 105346, 2021.
- [8] G. S. Arcanjo, A. H. Mounteer, C. R. Bellato, L. M. M. D. Silva, S. H. B. Dias, P. R. D. Silva, “Heterogeneous photocatalysis using TiO_2 modified with hydrotalcite and iron oxide under UV-visible irradiation for color and toxicity reduction in secondary textile mill effluent,” *J. Environ. Manage.*, vol. 211, pp. 154-163, 2018.